Amorphous Pt 1-x Ge x for Spintronics Applications: Growth and Characterization

Megumi Tanaka

Electrical Engineering and Computer Sciences
University of California, Berkeley

May 5, 2023

Acknowledgement

research advisor. Thank you for providing me with mentorship necessary to become a good researcher.

Finally, I would like to thank my friends and family for their support; I would not be here without them.

Contents

1 Introduction

1.1 Motivation

The development of cost-efficient, energy-efficient memory devices is of great interest. There is an urgent need for a large memory storage solution, which is simultaneously environmentally conscious. This project aims to optically measure the current-induced spin accumulation in amorphous (*a-*) Pt-Si and Pt-Ge films, with the goal to understand how the crystal structure, or more specifically the disordering of the structure of a material, affects the magnitude of the spin-Hall effect. This is of great practical interest, especially in applications in magnetic random-access memory (MRAM), which is considered the leading contender for a less expensive, lower power memory device of the future.

A novel memory storage device utilizing spintronics would create a pathway to drastically increased data storage, and ease environmental impacts through energy-efficiency, and in turn enable advancements in novel technologies that require high data processing speed. This would provide solutions to the limitations of data storage hindering computational performance, allowing society to see improvements and higher accessibility in medical, environmental, and educational technology.

1.2 Outline

This technical report is organized as follows: first we give some background on the Spin Hall Effect and prior research on amorphous materials in Section 2. For Section 3 we examine the fabrication and measurement methods such as film deposition, resistivity measurements, XRD, TEM, and AFM. In Section 4, we look at data that was acquired through the two fabrication and measurement cycles. Finally, the report will be concluded with final remarks and possible directions for future work.

2 Background

2.1 Spin Hall Effect

The spin-Hall effect (SHE) is a transport phenomenon that causes the accumulation of opposite spins on sides perpendicular to an electrical current in a nonmagnetic, conducting sample. By applying an electric current along an axis of a nonmagnetic material, electrons of opposite spins will migrate in opposite directions perpendicular to the current. In a "normal" sample, equal numbers of up and down spins means that no net flow vertical of charge exists, only a pure spin current. [1] Pt is known to have large SHE, and in turn the ability to produce large spin-orbit torque (SOT) on a neighboring ferromagnet. Both SHE and SOT are strongly dependent on spin-orbit coupling, as well as material properties such as mean free path and interface transparency, factors that are generally not well controlled. SHE is composed of an intrinsic and extrinsic component, both of which exist simultaneously in a material. The intrinsic component is based on the electronic structure of the material, while the extrinsic component arises from spin-dependent scattering from impurities [2].

2.2 Research on Amorphous Materials

There is potential for amorphous materials to create larger effects than its crystalline counterparts; for example, the magnetization and spin polarization at the Fermi surface and the anomalous Hall Effect (AHE) and anomalous Hall angle are all larger in amorphous Fe-Si and Fe-Ge alloys than in their crystalline states [3] and preliminary evidence suggests large SOT from non-magnetic low x a-Fe$_{1-x}$Si$_x$ [4]. This may be associated with the localization effects of the disorder which enhances the effect of spin-orbit coupling; this study will enable us to test this hypothesis by varying disorder separately from carrier concentration. Hellman Lab results show that the anomalous Hall conductivity is of order ten times larger in amorphous Fe-Si samples when compared to the crystalline counterparts [5]. Our group has also recently shown that the large AHE in ferromagnetic amorphous a-Fe-Ge can be calculated from DFT analysis and is the dominant contribution [3]. Intrinsic SHE has not yet been calculated for amorphous Pt alloys, but based on the AHE analog, is likely to be large and may be larger than in crystalline Pt.

Ge is a larger ion than Si, causing a narrowing of the bands and an enhanced density of states. It also has higher spin-orbit coupling (SOC) than Si. Thus a comparison of a-Pt$_{1-x}$Si$_x$ and a-Pt$_{1-x}$Ge$_x$ alloys, as well as varying x, allows for a separation of the effects of carrier density, from that of disorder. Amorphous Pt-Si and -Ge allows for controllability over composition, by changing the platinum-silicon or germanium ratio, which in turn changes the number of mobile electrons, while having a fixed mean free path unaffected by impurities due to the amorphous structure. This leads to the possibility of quantifying phenomena around the spin-Hall effect and spin-orbit torque.

3. Methods

3.1.1 Sample preparation

For all growths, amorphous SiN$_x$-on-Si substrates were used. The substrates were cleaned with a method where they were soaked in various organic solvents, in an order of decreasing volatility. First the substrates were soaked in acetone, after which the acetone was poured off, then rinsed with methanol, soaked in methanol, then the methanol was poured off, then soaked in isopropyl alcohol (IPA), and sonicated using the lab sonicator. All of the soaking and sonicating was conducted for 3-5 minutes. 9 samples were placed in a beaker, with care that they did not overlap each other in the bottom of said beaker. After the samples were cleaned, they were individually taken out of the beaker; each substrate was removed from the beaker using ultra-high vacuum (UHV) clean tweezers, and blown off with nitrogen gas from a compressed gas cylinder individually before being placed into a sample case, or mounted to the sample plate. For the growth of the Pt60Ge40 samples, one membrane substrate was also mounted onto the sample plate, in order to be measured via TEM (transmission electron microscopy). The small chips with 9 membrane TEM grids (each window is 0.1mm) require extra care when mounting, as clamping them similarly to regular Si substrates would shatter them. Once all substrates were mounted onto the sample plate, nitrogen gas was blown on the plate to remove dust particles,

with care to not blow directly onto the membrane TEM grids as they are easily shattered.

3.1.2 Film deposition

$Pt_{1-x}Ge_x$ films were grown by magnetron co-sputtering on 1cm x 1cm amorphous Si-N covered Si substrates, where x is between 0 and 0.4. Pt and Ge were codeposited, where the deposition rate is obtained from the crystal monitor through single-material deposition of Pt and Ge, then using a calculation method that determines growth times and power needed for each targeted composition. Two rounds of growths were done with the films being thicknesses of roughly 50 nm.

Sputtering is a process used for material deposition that involves bombarding a target material with high-energy ions, typically Argon, to dislodge atoms or molecules from the surface of the target. These atoms or molecules are then deposited onto a substrate to form a thin film. In sputtering, the target material is placed in a vacuum chamber and a plasma is created using a gas, in this case argon. The plasma is then used to bombard the target material with high-energy particles, causing atoms or molecules to be ejected from the target surface. These ejected particles then travel through the vacuum chamber and are deposited onto the substrates.

3.2 Resistivity measurements

Resistivity of samples vs temperature was measured using the lab closed cycle system. This system allows the temperature of the sample to be controlled, from 2 to 300K, in a vacuum environment, with multiple electrical feedthroughs to enable application of a current to the sample, and measurement of the voltage across the sample and its temperature. The four-point measurement method is used to eliminate any contact resistance, and involves placing four electrodes on the sample, typically at the corners of a square or rectangle. A current is applied between two adjacent electrodes. The voltage drop across the other two electrodes is measured, and the process is repeated with the current applied between the other pair of adjacent electrodes. By measuring the voltage drop across two pairs of electrodes, one can determine the resistivity of the sample.

It is a non-destructive method and can be used to study the properties of the material as a function of temperature, magnetic field, and other parameters. Data taken from the measurements was calculated via the van der Pauw method, which measures the voltage and current at different pairs of contacts on the sample and uses this data to calculate the resistivity and of the material.

The van der Pauw equation relates the resistance of a thin sample to the two measured voltages and current data. The equation is given as:

$$R = (\frac{1}{I\pi})(\ln(\frac{4R_0}{R_1}) + (\ln\frac{4R_0}{R_2}))$$

where R is the resistance of the sample, I is the current flowing through the sample, R_0 is a reference resistance, and R_1 and R_2 are the resistances measured between different pairs of contacts on the sample. The reference resistance R_0 is typically chosen to be large enough so that it dominates the measured resistance. [6]

Conductivity (σ) expresses how easily a material can conduct electric current, while resistance (R) is the ratio between the voltage applied, and the current flowing through it. Conductivity and resistivity (ρ) are inversely related, and resistance is directly proportional to resistivity and length, but inversely proportional to cross-sectional area. The relationships can be expressed as follows:

Conductivity and resistivity: $\sigma = \frac{1}{\rho}$

Resistance and resistivity: $R = \frac{\rho L}{A}$

where L is the length of the material, A is the cross-sectional area, and ρ is the resistivity of the material.

The specific system used in this project is a dry benchtop cryostat, the Janis closed cycle refrigerator (CCR) system. It provides a convenient means of cooling samples to temperatures below 10 K in vacuum, and can be used to perform a wide variety of optical and electrical experiments between ~8 K and 325 K (475 K optional). By being fitted with a heater, the warming process is accelerated from the cooling process, and measurements above room temperature can be conducted. CCR systems require no liquid helium or liquid nitrogen as a source of cooling. Instead, a closed loop of helium gas is compressed and expanded using the compressor below the bench, manufactured by Sumitomo. During the expansion phase of each cycle, heat is removed from the cold finger, on which the sample is mounted. (A detailed description of the G-M cycle can be found on page C-3 in the refrigerator manual). A heater and thermometer are installed on the cold finger and are used to precisely control the sample temperature. [7]

The sample stage inside the cryostat has eight pins, to which fine wires were soldered and re-used for up to two simultaneous resistivity measurements. Samples were attached to the stage using GE varnish, and sample contacts were made by attaching indium to the sample corners, placing the wire on the indium, then securing the wire by placing another small piece of indium on top ("indium sandwich technique"). DC resistivity measurements for this work were taken using a Keithley 2400 sourcemeter controlled by a GUI Python program [5]

3.3 XRD

X-ray diffraction (XRD) is a measurement technique used to study the structure of crystalline materials. A beam of X-rays is directed at a sample, which causes the X-rays to diffract or scatter in various directions, depending on the arrangement of atoms in the sample. By analyzing the diffraction pattern, the spatial arrangement of atoms in the sample, as well as the crystal structure and orientation can be determined. For this project, XRD measurements were made in order to observe broadening of the Pt peak as percent Si increases.

The XRD measurement setup consists of an X-ray source, sample holder, and detector. The X-ray source emits a beam of X-rays, which is collimated and directed onto the sample. The X-ray beam is directed at it from various angles, and scattered X-rays are detected by the detector. The resulting diffraction pattern is recorded as a plot of intensity versus angle, known as a diffraction pattern.

The diffraction pattern is analyzed to determine the crystal structure of the sample. This is typically done by comparing the measured diffraction pattern to a database of known diffraction patterns for different crystal structures. By finding the best match between the measured pattern and the database patterns, the crystal structure and orientation of the sample can be determined.

The angles of the interference maxima in a measured XRD pattern can be correlated to a database of X-ray diffraction data to deduce the crystal structure of a sample. If no peaks are observed in the diffraction pattern, then the sample may be amorphous; however, the sample may also be nano-crystalline with crystallites too small to observe with the wavelength of X-rays used, and it is impossible to know from XRD alone which of these structures exists in a sample. In other words, the absence of sample peaks in the XRD pattern is a necessary but not sufficient condition to prove sample amorphicity. So, to avoid any misleading implications, XRD patterns of "amorphous" materials will not be shown in this work and we will instead use transmission electron microscopy (Sec. 2.2.2) as proof of amorphicity. [3]

3.4 TEM

Tunneling Electron Microscopy (TEM) is a technique for imaging and analyzing the surface structure of materials at the atomic scale. TEM is the method used in this project to determine sample amorphicity. Measurements are based on interference of energetic electrons that have been deflected by the electrostatic fields within a material. Samples measured by TEM must be grown onto a silicon nitride TEM membrane, and the total sample thickness must be limited.

TEM works based on the principle of quantum tunneling, which is the phenomenon where a particle can pass through a potential barrier even if it doesn't have enough energy to overcome it. In TEM, a beam of electrons is directed towards the surface of the sample. As the electrons approach the surface, some of them are reflected back, while others tunnel through the surface barrier and form an image on a detector. For a crystalline material, the electron diffraction pattern

consists of spots where the spacing and orientation is determined by the crystal structure, as well as the orientation relative to the electron beam. The absence of any nanocrystalline phase in the diffraction pattern can be confirmed via a TEM image, and an HRTEM (high-resolution transmission electron microscopy) image that shows highly disordered structure without any sign of nanocrystals or ordered clusters can confirm an amorphous structure.

3.5 AFM

Atomic force microscopy (AFM) is a technique used to measure surface features and topography at the nanometer scale. Before an AFM measurement, the sample must be clean and free of any contamination or debris that may interfere with the measurement. The surface should also be as smooth and flat as possible.

AFM consists of a sharp tip that is approximately 10 to 20 nm in diameter, which is attached to a cantilever. AFM tips and cantilevers are micro-fabricated from Si or Si_3N_4. The tip moves in response to tip–surface interactions, and this movement is measured by focusing a laser beam with a photodiode.

An AFM is operated in two basic modes, contact and tapping modes. In the contact mode, the AFM tip is in continuous contact with the surface. In contrast, in the tapping mode, the AFM cantilever is vibrated above the sample surface such that the tip is only in intermittent contact with the surface. This process helps to reduce shear forces associated with the tip movement. The tapping mode is the recommended mode that is commonly used for AFM imaging. The contact mode is only used for specific applications, such as force curve measurements. The AFM is used to image and manipulate atoms and structures on a variety of surfaces. The atom at the apex of the tip 'senses' individual atoms on the underlying surface when it forms incipient chemical bonds with each atom. Because these chemical interactions delicately alter the tip's vibration frequency, they can be detected and mapped. [8]

AFM images can be used to calculate surface roughness, which is an important parameter for many materials applications. The root mean square (RMS) roughness and the average roughness (Ra) are commonly used metrics for roughness analysis. Step height (differences in surface height between adjacent regions), fractal analysis (quantifies the self-similarity of surface features at different length scales), and surface potential mapping (measure electrostatic forces between the AFM tip and the sample surface) can be derived from AFM measurements.

4 Results

4.1 Film deposition
Two growths were done, and this report will focus on the results of the measurements made on the first growth. The sample growths made for the first batch were named as follows; S22005 (Pt100), S22006 (Pt90Ge10), S22007 (Pt80Ge20), S22008 (Pt70Ge30), S22009 (Pt60Ge40). For the second growth, the samples were named as follows; S22060 (Pt100), S22061 (Pt90Ge10), S22062 (Pt80Ge20), S22066 (Pt70Ge30), S22069 (Pt60Ge40). For sample growths S22009 and S22069, sputtering was done onto Si substrates as well as membranes to be measured via TEM. The first batch of samples were measured on closed cycle, XRD, TEM (for S22009), and AFM, but only XRD measurements were done on the second batch of samples.

4.2 Resistivity measurements
Four point resistivity measurements were taken at temperatures from roughly 290K to 4K, for one sample from each growth. The resistivity values for each sample taken at room temperature are below.

S22005	164.34μΩ*cm
S22006	252.6μΩ*cm
S22007	691.50μΩ*cm
S22008	1574.28μΩ*cm
S22009	2696.34μΩ*cm

The figures below show the relationship between resistivity and composition (%Ge) (Fig. 1), and the relationship between conductivity and composition (Fig. 2), both measured at 5K. A trend of increasing resistivity, and decreasing conductivity with increasing Ge percentage can be observed. With increased Ge (semiconductor) concentration, the carrier density is decreased, and with increased Ge concentration also leads to increased resistivity and changes temperature dependence, diluting Pt (metal). This also reduces the grain size, which reduces the carrier mean free path and hence increases resistivity, but once amorphous, the grain size would not contribute to any changes in resistivity. In Fig. 3, only Pt60Ge40 expresses decreasing resistivity with increasing temperature, which is distinctly different from the other concentrations. As resistivity drops with increasing temperature, that is a signifier of carrier density dominating the resistivity change; if this sample was a metal, the carrier density would not change, thus this sample is expressing a likeness to the semiconducting regime.
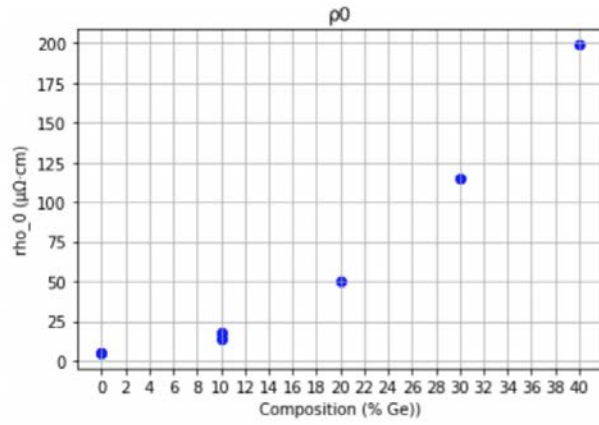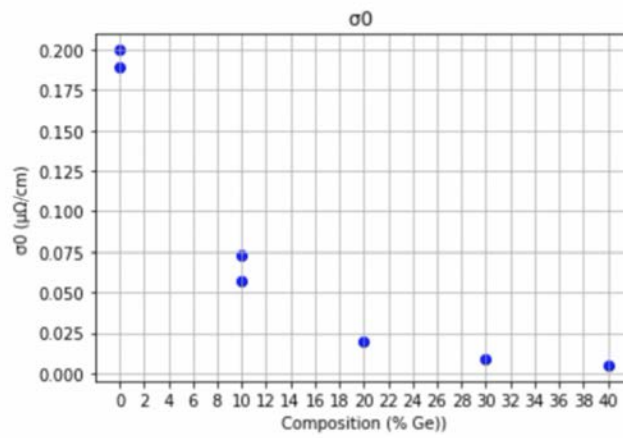
Fig. 1

Fig. 2

Fig. 3 shows the 4-point resistivity vs temperature measurements. Increasing resistivity across all temperatures can be observed for all samples, with increasing Pt composition. Pt100 sample shows a negative slope, with increasing resistivity with decreasing temperature.
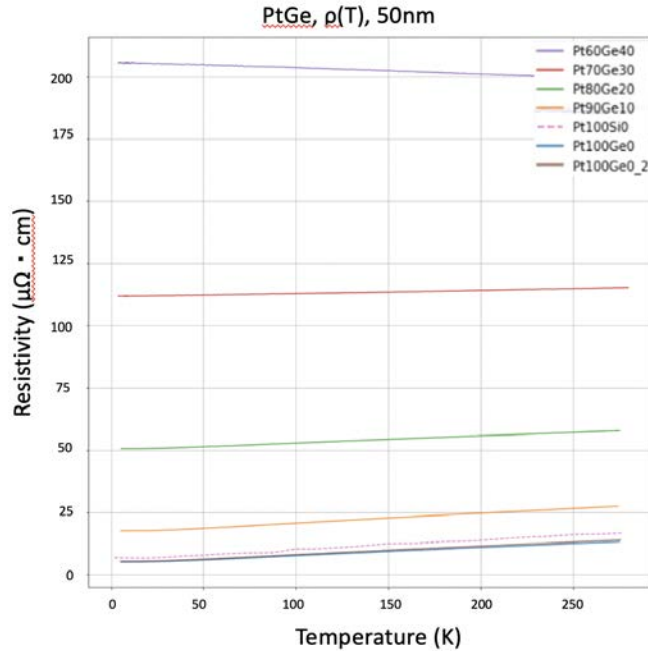
Fig. 3

Fig. 4 shows the resistivity measurements offset by resistivity at 5K. This is done in order to compare the rate of the resistivity change per temperature increase. The slope of each curve decreases with increasing Si percentage, except for Pt90Ge10 and Pt100 where Pt100 has a lower resistivity than Pt 90 at.%. It is possible that the samples were switched prior to the measurement, as measuring the same samples twice yielded marginal changes. It could also be hypothesized that there is competition of domination occurring between the effects of mean free path and carrier density. Additionally, Pt 60 at.% has a negative slope, which shows increasing resistivity with decreasing temperature, expressing a large resistivity change between the Pt60 and Pt 70 at.% samples. For Pt 60 at.%, increasing resistivity with decreasing temperature shows semiconducting properties, moving away from the pure metal properties. In a pure metal, lower resistivity would be expressed with lower temperature, due to having less carriers able to move above the bandgap. From the TEM data (expressed in part 4.4), we are able to conclude that Pt60Ge40 is an amorphous sample. From Fig. 4 we can see the slope of resistivity vs temperature for Pt60 is negative, and this change in sign shows that the carrier density fully dominates in this regime. Structural phase transitions are observed at Pt 60 at.%, and we also see carrier density dominate the transport signature at said concentration. Once amorphous, the mean free path no longer has an effect on resistivity change, therefore carrier density dominates the transport signature. Since it is known from TEM data that the Pt 60 at.% sample is amorphous, the transport signature would no longer be dominated by grain size, and mean free path no longer depends on temperature
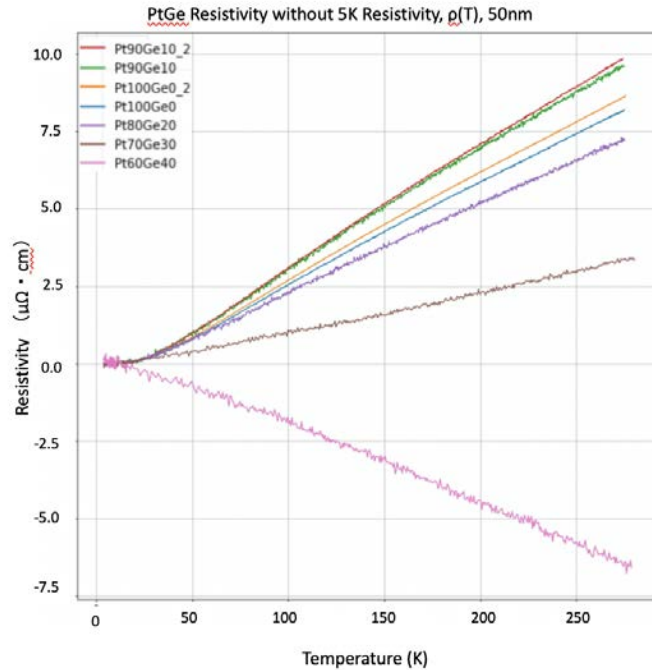
Fig. 4

4.3 XRD

Fig 5~9 shows the first batch of samples when measured with the same XRD parameters (38-41 degree scan width, step size 0.02, time per step 200 seconds, net run time 8:26:58). It can be observed that the peak intensity decreases with increased Ge concentration, except for Pt 70 at.% and Pt 80 at.% where Pt 70 at.% has an unexpected higher intensity peak than Pt 80 at.%. In the scan shown in the graph, no peak can be observed in the Pt 60 at.% sample; this is significant as the change between Pt 70 at.% and Pt 60 at.% scans indicates that there is a transition in crystallization somewhere between those concentrations.. Pt 70 at.%, Pt 80 at.%, Pt 90 at.%, Pt 100 at.% samples all show polycrystalline properties by showing a peak. For the second batch of growths, the samples were labeled in a strict manner, and care was taken to not switch up the samples. That said, although we would expect the peak to drop as a function of increasing Ge concentration, that is not the case at Pt 80 at.% and Pt 70 at.%. It can be hypothesized that there is an issue of composition segregation at these two compositions occuring, where the Pt is not homogeneously distributed. Since XRD measurements are dominated by heavier elements by a factor of Z^3, scattering from Pt would dominate. The Pt60Ge40 sample here shows no visible peak, and it can be hypothesized that the sample is amorphous at this point. Additionally, Pt60Ge40 composition was confirmed to be amorphous in section 4.4. The crystallization process happens during growth in the other composition samples, and there are no post-temperature treatments done to these samples.
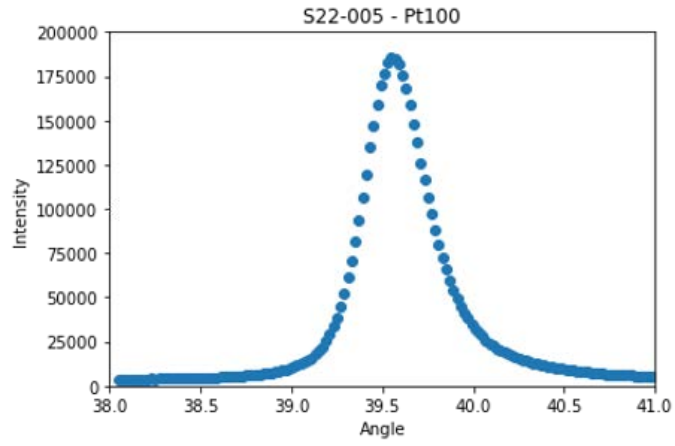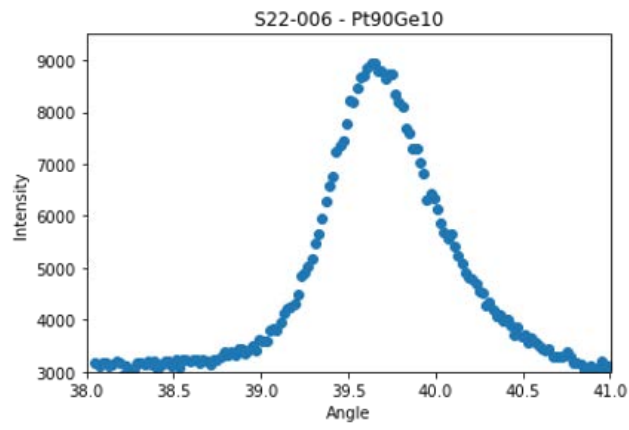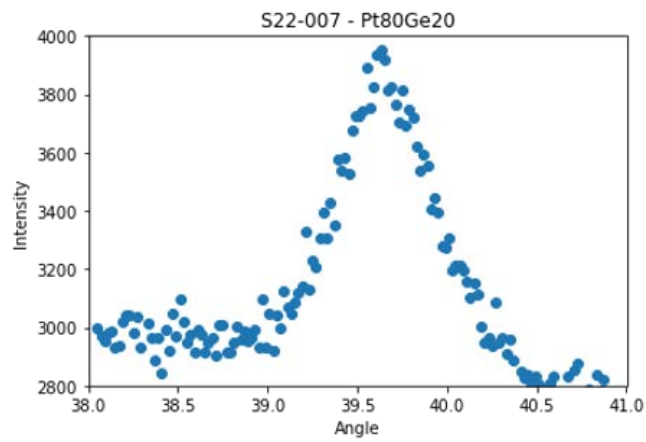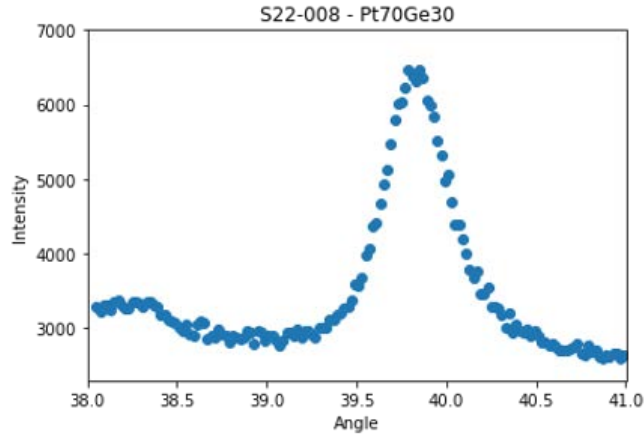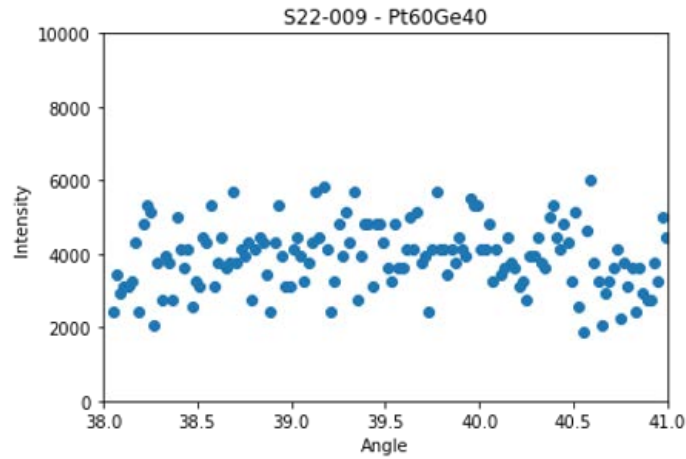
Fig. 5

Fig. 6

Fig. 7

Fig. 8

Fig. 9

Fig 10 shows XRD scans in log scale that were performed on the second batch of samples S22060 (Pt100), S22061 (Pt90Ge10), S22062 (Pt80Ge20), S22066 (Pt70Ge30), S22069 (Pt60Ge40), and here also a higher peak can be observed in Pt 70 at.% compared to Pt 80 at.%. Here too, it can be hypothesized that there is an issue of composition segregation at these two compositions occuring, where there is more Pt at the top of the film, and is not homogeneously distributed throughout the film. The Pt 60 at.% sample here shows no visible peak, and can be hypothesized that the sample is amorphous at this point. However, TEM measurements were not able to be conducted on this batch of samples, and therefore conclusions on amorphicity cannot be made from XRD diffraction pattern alone. It is possible that the sample is nanocrystalline with crystallines that are too small to be observed by the X-ray wavelength, and until confirmed with TEM measurement, a sample not showing a peak is not necessarily amorphous.
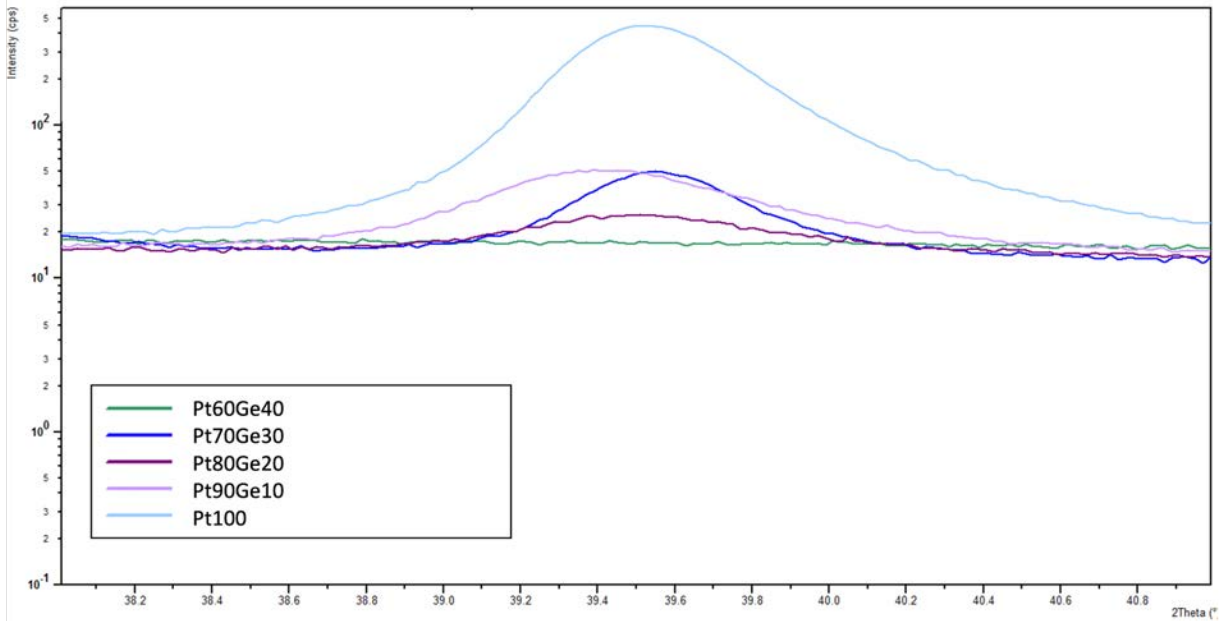
Fig. 10

4.4 TEM

Fig. 11 and Fig. 12 show TEM measurement of a membrane grown in the S22009 (Pt60Ge40) growth. From the top-down TEM image in Fig.11, we cannot see any lattice fringes. The fast-fourier transform image of the TEM image also shows a continuous ring, which indicates a fully amorphous ring. Select area electron diffraction (SEAD) shows no peak (Fig.12), which indicates an amorphous sample. We would see spots on the SEAD image, if otherwise. The next step would be to measure Pt80Ge20 and Pt70Ge30 via TEM. The XRD peaks for these samples show that they are both at least partially crystallized. TEM would show if these two samples are a mix of amorphous and nanocrystals, or purely nanocrystalline.

Fig. 11

Fig. 12

4.5 AFM

AFM measurements were done on Pt100, Pt90Ge10, and Pt80Ge20 samples made in the second batch.

Fig 13 and 14 show AFM measurements of a Pt80Ge20 sample. Fig 13 shows the analysis of the impurities and contaminants on the surface, which is a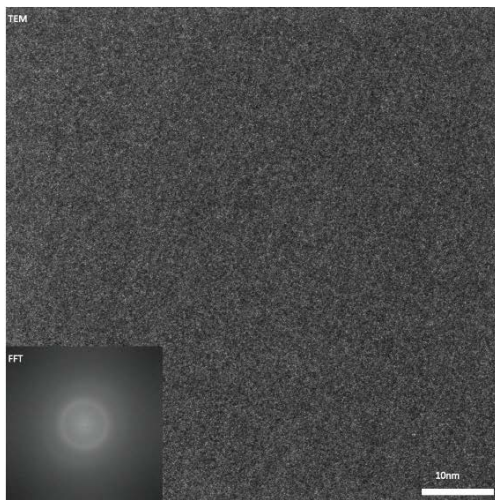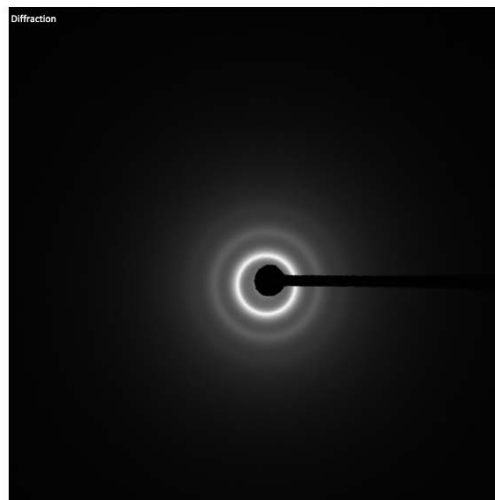 necessary step to attain Fig 14, which analyzes the region of interest. After filtering out the impurities on the surface via the AFM data acquisition software ("masking out" the impurities), as seen in Fig. 14, the film surface roughness without impurities are measured. As the RMS in Fig. 14 is less than 0.3nm, it can be concluded that the film is relatively smooth. An AFM measurement with parameters of 100 nm x 100 nm would perhaps have a scan area small enough to show grain size, but the scans conducted in this measurement were not sufficient in resolution to make significant conclusions about grain size.

Stats	Full Image	Masked Image
RMS	563.575 pm	3.014 nm
Sdev [Rq]	563.579 pm	1.132 nm
Adev [Ra]	296.679 pm	884.220 pm
Max	8.266 nm	8.266 nm
Min	-4.329 nm	1.364 nm
Avg	0.000 m	2.794 nm
Skew	4.23	1.24
Kurt	33.3	2.19
Percent	100.0%	2.3%
Area	25.0 µm²	390362.3 nm²
Area %	0.02351%	0.3541%
Volume	0 m³	0.0016 µm³

Fig. 13

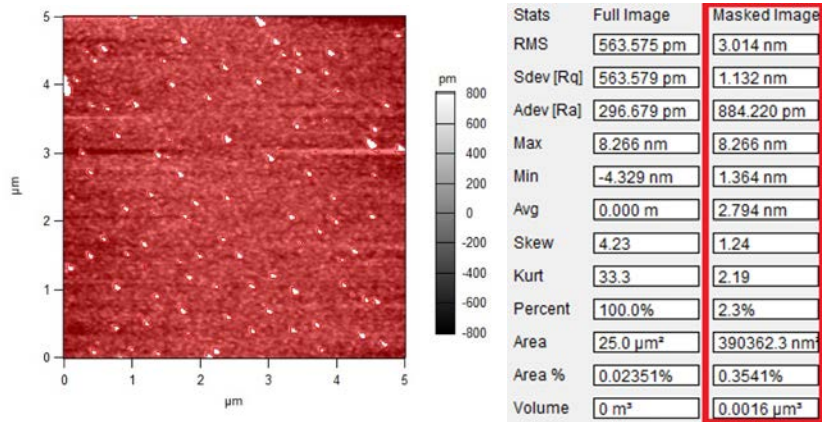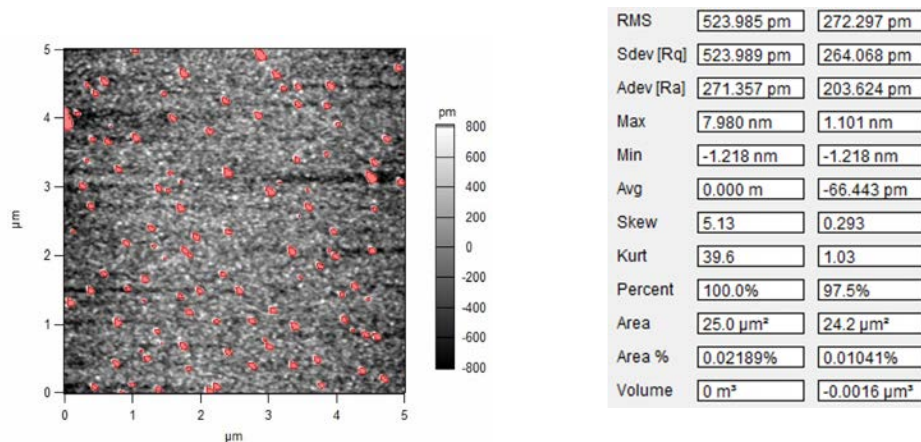| RMS	523.985 pm	272.297 pm
Sdev [Rq]	523.989 pm	264.068 pm
Adev [Ra]	271.357 pm	203.624 pm
Max	7.980 nm	1.101 nm
Min	-1.218 nm	-1.218 nm
Avg	0.000 m	-66.443 pm
Skew	5.13	0.293
Kurt	39.6	1.03
Percent	100.0%	97.5%
Area	25.0 µm²	24.2 µm²
Area %	0.02189%	0.01041%
Volume	0 m³	-0.0016 µm³

Fig. 14

For Fig. 15, a Pt90Ge10 sample was measured. The same conclusion can be drawn from that of the Pt80Ge20 sample, where the RMS is relatively small and the surface is relatively flat.

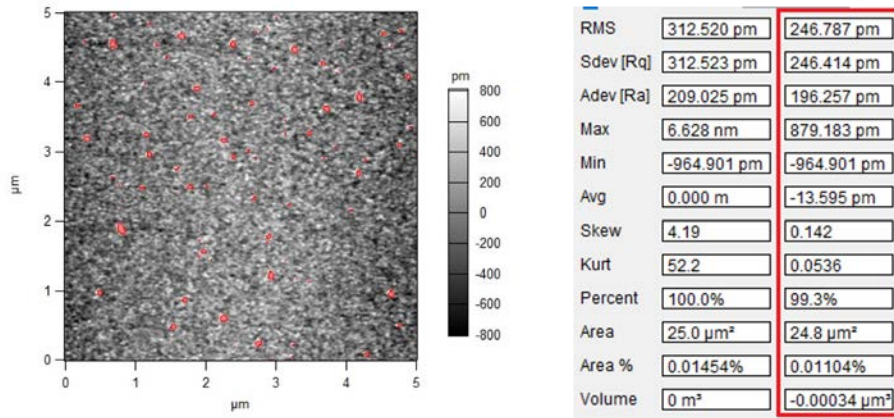|		
RMS	312.520 pm	246.787 pm
Sdev [Rq]	312.523 pm	246.414 pm
Adev [Ra]	209.025 pm	196.257 pm
Max	6.628 nm	879.183 pm
Min	-964.901 pm	-964.901 pm
Avg	0.000 m	-13.595 pm
Skew	4.19	0.142
Kurt	52.2	0.0536
Percent	100.0%	99.3%
Area	25.0 µm²	24.8 µm²
Area %	0.01454%	0.01104%
Volume	0 m³	-0.00034 µm³

Fig. 15

For Fig. 16, a Pt100 sample was measured. It can be observed that the surface roughness is higher than that of the other samples. Pt films have been previously observed to have large crystals, which lead to greater roughness. Ge serves as nucleation sites and creates potentially smaller grains and increased numbers, allowing for a sample that is closer to an amorphous state, which would have a very smooth surface.

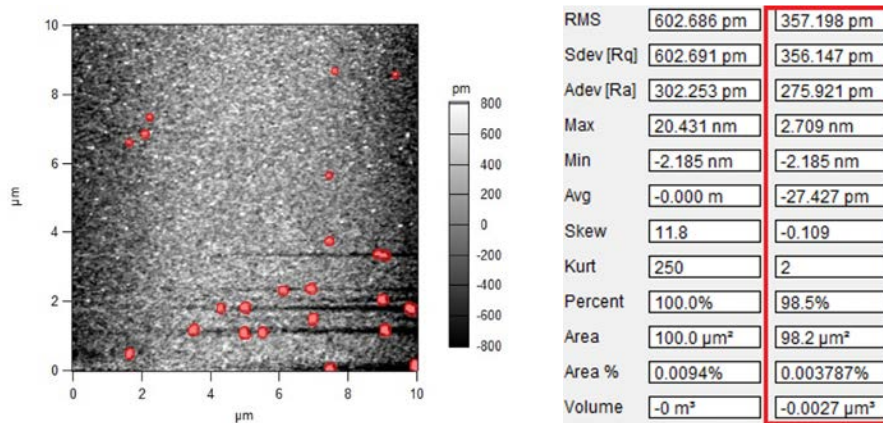|		
RMS	602.686 pm	357.198 pm
Sdev [Rq]	602.691 pm	356.147 pm
Adev [Ra]	302.253 pm	275.921 pm
Max	20.431 nm	2.709 nm
Min	-2.185 nm	-2.185 nm
Avg	-0.000 m	-27.427 pm
Skew	11.8	-0.109
Kurt	250	2
Percent	100.0%	98.5%
Area	100.0 µm²	98.2 µm²
Area %	0.0094%	0.003787%
Volume	-0 m³	-0.0027 µm³

Fig. 16

5 Conclusion and Future Works

In conclusion, it can be observed that Ge 40 at.% is likely the critical concentration where the structure of Pt transitions to a fully amorphous phase. This can be assumed from the S22009 sample showing amorphous properties in the TEM measurement, and the sample also lacks a peak in the XRD measurements. For future work, films could be structurally characterized via methods such as XRD, HRTEM, AFM and compositionally via RBS (Rutherford backscattering spectrometry_ and XPS (X-ray photoelectron spectroscopy), and electronically by resistivity and Hall effect vs. temperature via measurements with a Cryostat with a magnet. By creating amorphous Pt through doping with varying levels of Si and separately Ge from 0-50at.%, and creating samples of varying compositions on membranes to be measured with TEM, the effect of atomic disorder on spin-accumulation from the spin-Hall effect and on SOT can be studied in correlation to amorphicity and to electron mean free path, from ordinary hall effect and resistivity, and grain size. By creating amorphous Pt through doping with varying levels of Ge from 0-40at.%, the effect of atomic disorder on spin-accumulation from the spin-Hall effect and on SOT can be studied as future works. The proposed method for measuring SHE, specifically the current-induced spin accumulation of amorphous Pt-Si and Pt-Ge, is by use of second harmonic imaging MOKE (Magneto-optic Kerr effect). This technique is able to probe the surface spin accumulation with time sensitivity on the sub-nanosecond scale from short current pulses [9]. To characterize the SOT, harmonic Hall measurements of effective magnetic fields by using a neighboring Co layer will need to be conducted, a process which will require patterning.

References

[1] Sinova, J., Valenzuela, S. O., Wunderlich, J., Back, C. H., & Jungwirth, T. (2015). Spin Hall effects. *Reviews of Modern Physics*, *87*(4), 1213–1260.

[2] Amin, V. P., Haney, P. M., & Stiles, M. D. (2020). Interfacial spin–orbit torques. *Journal of Applied Physics*, *128*(15), 151101.

[3] Karel, J., Bouma, D. S., Fuchs, C., Bennett, S., Corbae, P., Song, S. B., Zhang, B. H., Wu, R. Q., & Hellman, F. (2020). Unexpected dependence of the anomalous Hall angle on the Hall conductivity in amorphous transition metal thin films. *Physical Review Materials*, *4*(11), 114405.

[4] Hsu, C.-H., Karel, J., Roschewsky, N., Cheema, S., Bouma, D. S., Sayed, S., Hellman, F., & Salahuddin, S. (2020). Spin-orbit torque generated by amorphous Fe_xSi_{1-x}. *arXiv:2006.07786*

[5] Bouma, D. S., Chen, Z., Zhang, B., Bruni, F., Flatté, M. E., Ceballos, A., Streubel, R., Wang, L.-W., Wu, R. Q., & Hellman, F. (2020). Itinerant ferromagnetism and intrinsic anomalous Hall effect in amorphous iron-germanium. *Physical Review B*, *101*(1), 014402.

[6]van der Pauw, L. J. A method of measuring specific resistivity and Hall effect of discs of arbitrary shape. Philips Res. Rep. 13, 1–9 (1958).

[7] *Janis Closed Cycle Refrigerator System Manual*. (n.d.).

[8] Ray, S. S. (2013). *Environmentally friendly polymer nanocomposites*. Woodhead Publishing

[9] Pattabi, A., Gu, Z., Gorchon, J., Yang, Y., Finley, J., Lee, O. J., Raziq, H. A., Salahuddin, S., & Bokor, J. (2015). Direct optical detection of current induced spin accumulation in metals by magnetization-induced second harmonic generation. *Applied Physics Letters*, *107*(15).